Methodology of numerical coupling for transient conjugate heat transfer

E. Radenac [a,*], J. Gressier [b], P. Millan [a]

[a] Onera, The French Aerospace Lab, F-31055 Toulouse, France
[b] Institut Supérieur de l'Aéronautique et de l'Espace, 10 av. Edouard Belin, BP 54032, 31055 Toulouse, France

ARTICLE INFO

Keywords:
Conjugate heat transfer
Coupling
Finite Volume Method
Conservativity
Accuracy
Verification

ABSTRACT

This paper deals with the construction of a conservative method for coupling a fluid mechanics solver and a heat diffusion code. This method has been designed for unsteady applications.

Fluid and solid computational domains are simultaneously integrated by dedicated solvers. A coupling procedure is periodically called to compute and update the boundary conditions at the solid/fluid interface. First, the issue of general constraints for coupling methods is addressed. The concept of interpolation scheme is introduced to define the way to compute the interface conditions. Then, the case of the Finite Volume Method is thoroughly studied. The properties of stability and accuracy have been optimized to define the best coupling boundary conditions: the most robust method consists in assigning a Dirichlet condition on the fluid side of the interface and a Robin condition on the solid side. The accuracy is very dependent on the interpolation scheme. Moreover, conservativity has been specifically addressed in our methodology. This numerical property is made possible by the use of both the Finite Volume Method and the corrective method proposed in the current paper. The corrective method allows the cancellation of the possible difference between heat fluxes on the two sides of the interface.

This method significantly improves accuracy in transient phases. The corrective process has also been designed to be as robust as possible. The verification of our coupling method is extensively discussed in this article: the numerical results are compared with the analytical solution of an infinite thick plate in a suddenly accelerated flow (and with the results of other coupling approaches).

1. Introduction

Many industrial applications are subject to strong thermal interactions between fluids and solids. Severe configurations exhibit intense aerothermal phenomena, involving complex flows and geometries, unusual thermal conditions at their boundaries and multiple fluids and solids.

Conjugate heat transfer is thus a key industrial issue which can be investigated in several ways. Analytical approaches produce interesting information to identify the leading parameters of a problem and to verify codes. But their applicability is restricted to very simple configurations (such as forced convection over an infinite or semi-infinite thick plate [1,2] or in a channel with thick walls [3]). Alternatively, experiments are essential at least for validation (for instance, the study reported in paper [4]). But they are expensive. The development of new technologies thus cannot rely only on experiments.

That is why numerical simulations are absolutely necessary. For a long time, they have consisted of decoupled studies. For instance, numerical flow simulations were performed with given thermal boundary conditions (often adiabatic or isothermal). This approximate method does not account for the fact that convection affects the fields of temperature and heat fluxes in the solid. There is an essential condition for computing both fluid and solid parts accurately. At their interface, the boundary conditions must be properly calculated.

Coupled methods are therefore necessary for conjugate heat transfer. There is a particular need for unsteady studies. For example, in the aeronautical industry, several transient phases occur in a jet engine during a flight. The safety margins are usually set by steady-state approaches. They could be reduced by a better characterization of transient phenomena.

Sondak et al. [5] have noticed that many studies mainly produce steady-state results for aerothermal fields in turbines [6–10]. Several solver couplings are also dedicated to very specific configurations, with specific geometries or solvers (studies in the fields of space [11], combustion [12,13]). Besides, more and more unsteady applications can be found in the literature [5,12–15,21].

Sometimes, the whole computation uses a single fluid solver which treats solid parts as rigid bodies. But it is usual to couple distinct fluid and solid solvers. The fluid and solid domains are

* Corresponding author.
E-mail addresses: emmanuel.radenac@onera.fr (E. Radenac), jeremie.gressier@isae.fr (J. Gressier), pierre.millan@onecert.fr (P. Millan).

integrated by separate solvers or procedures which periodically exchange data.

The method proposed in the current paper is intended to be appropriate for unsteady computations and to ensure robustness, accuracy and conservativity. This has implied a choice among methodological options widely discussed in the literature (sequential or parallel coupling strategy, nature of the boundary condition at the interface for the different solvers).

In terms of accuracy, the coupling methodology affects unsteady calculations more than steady-state simulations. Most coupling methods do not ensure the proper instantaneous conditions at the solid/fluid interface. This issue will be extensively discussed in the current article. The innovative concept of interpolation scheme will be introduced. A novel interpolation scheme will be proposed and compared to more usual approaches of the literature.

Moreover, our coupling methodology is intended to be conservative. This concept is poorly discussed in the literature of coupling strategies. Conservativity ensures that no energy is lost during the computation. This requires the use of the original method described in this paper. It will be demonstrated that a conservative method improves accuracy even though the codes exchange data at small frequencies, which leads to gains in computational cost. A verification case will show the efficiency of our method.

2. Physical problem

This section presents the main equations describing heat transfer in a solid, in a fluid and at their interface. In the whole paper, the subscripts I, S and F will denote the properties at the interface, in the solid and in the fluid, respectively.

2.1. Conservation laws and heat transfer in solids and fluids

Solids and fluids are governed by conservation laws in the general form

$$\frac{\partial U}{\partial t} + \overrightarrow{\nabla}(\vec{F}(U)) = \mathbb{S}, \tag{1}$$

where U is a vector of conserved quantities, $\vec{F}$ is a flux tensor and $\mathbb{S}$ is a vector of source terms.

2.1.1. Heat transfer in solids

For solids, $U = e_S, \vec{F} = \overrightarrow{\Phi}_S$ and $\mathbb{S} = \rho_S \Phi_{\tau,S}$, where the internal energy e_S depends on the temperature $T_S : e_S = \rho_S c_S T_S$. The heat flux density is given by Fourier's law $\overrightarrow{\Phi}_S = -\lambda_S \cdot \overrightarrow{\nabla} T_S$. $\Phi_{\tau,S}$ is a heat source. ρ_S, c_S and λ_S are the mass density, the specific heat capacity and the thermal conductivity of the material, respectively.

2.1.2. Heat transfer in fluids

For fluids, Eq. (1) represents the Navier–Stokes equations [16]. Heat transfer is more specifically described by the law of conservation of energy

$$\frac{\partial \rho_F e_F}{\partial t} + \mathrm{div}(\rho_F e_F \overrightarrow{V}_F - \overrightarrow{\overrightarrow{\Sigma}}_F \cdot \overrightarrow{V}_F + \overrightarrow{\Phi}_F) - \rho_F \overrightarrow{\mathcal{F}}_F \cdot \overrightarrow{V}_F - \rho_F \Phi_{\tau,F} = 0, \tag{2}$$

where the total energy of the fluid is given by $e_F = \frac{r}{\gamma - 1} T_F + \frac{\overrightarrow{V}_F^2}{2}$. Thus, heat transfer involves convection ($\mathrm{div}(\rho_F e_F \overrightarrow{V}_F)$), a heat source due to viscous effects (included in $\mathrm{div}(-\overrightarrow{\overrightarrow{\Sigma}}_F \cdot \overrightarrow{V}_F)$), heat diffusion ($\mathrm{div}(\overrightarrow{\Phi}_F) = \mathrm{div}(-\lambda_F \overrightarrow{\nabla} T_F)$) and other heat sources ($\rho_F \Phi_{\tau,F}$). $\overrightarrow{V}_F, \rho_F$ and T_F are the flow velocity, the fluid density and the temperature, respectively. λ_F is the thermal conductivity, r is the specific gas constant and γ is the heat capacity ratio. $\overrightarrow{\mathcal{F}_F}$ represents the body forces (for instance gravity), $\overrightarrow{\overrightarrow{\Sigma}}_F$ is the stress tensor.

2.2. Solid/fluid interface

Under the assumption of perfect thermal contact, normal heat flux and temperature are continuous across the interface between a solid and a fluid. The heat flux condition $\Phi_I = \overrightarrow{\Phi}_I \cdot \vec{n}$ ($\vec{n}$ is the surface normal, here oriented from the solid to the fluid) and the temperature condition T_I at the interface should thus be such that

$$\begin{aligned} \Phi_I &= \Phi_{I,S} = -\Phi_{I,F}, \\ T_I &= T_{I,S} = T_{I,F}, \end{aligned} \tag{3}$$

where the subscripts $_{I,S}$ and $_{I,F}$ have been introduced to indicate conditions right at the interface on the solid and fluid sides, respectively (see Fig. 1 in the case of the Finite Volume Method). Here, the heat flux vector $\overrightarrow{\Phi}_{I,S}$ is oriented from the solid to the fluid (whereas conversely, $\overrightarrow{\Phi}_{I,F}$ leaves the fluid).

During the independent integrations of the solid and fluid domains, the solvers do not enforce both temperature and heat flux at their interface. Therefore, Eq. (3) cannot always be satisfied. Coupling a fluid solver and a solid solver consists of periodically updating their interface boundary condition so that the heat flux Φ_I and the temperature T_I fulfil condition (3) at each face of the interface. The numerical evaluations of Φ_I and T_I actually depend on temperature and heat flux in the solid and fluid domains (T_S, T_F, Φ_S and Φ_F, respectively) and on other parameters such as the solid and fluid heat conductances (h_S and h_F, which will be more precisely defined in Section 4.1.1):

$$\begin{cases} \Phi_I = \mathcal{F}_\Phi(\Phi_S, \Phi_F, T_S, T_F), \\ T_I = \mathcal{F}_T(\Phi_S, \Phi_F, T_S, T_F). \end{cases} \tag{4}$$

$\mathcal{F} = (\mathcal{F}_\Phi, \mathcal{F}_T)$ will be called an interpolation scheme. At this stage, it is not specified where exactly T_S, T_F, Φ_S and Φ_F are assessed. For temperature specifically, T_S and T_F may be assessed either at the interface or at the neighboring node (or at the centroid of the neighboring cell).

3. General coupling strategy

In this section, the main properties of our coupling strategy will be described independently of the discretization technique used in the coupled solvers. Section 4 will deal with the application of this strategy to the Finite Volume Method.

3.1. Coupling process

Several strategies can be employed to couple fluid and solid solvers. Duchaine [15] has proposed to distinguish between sequential (Fig. 2) and parallel coupling strategies (Fig. 3).

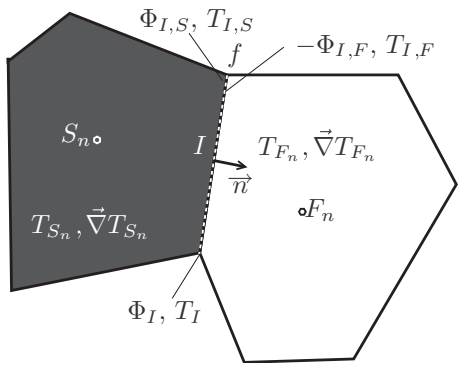

Fig. 1. Adjacent cells in the vicinity of a coupling interface.

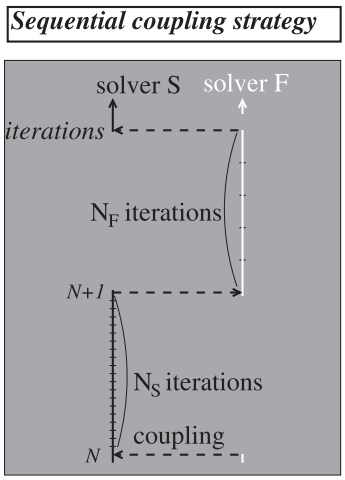

Fig. 2. Sequential coupling strategy.

In the sequential approach, the solid and fluid solvers are run alternately, each of them providing the boundary condition of the other. In the example of Fig. 2, at coupling step N, the fluid code provides a boundary condition to the solid solver. The solid domain is then integrated during N_S iterations. At the following synchronization, the fluid solver receives data from the solid solver, allowing to solve the fluid domain. The sequential coupling strategy is quite easy to implement, because the solvers are successively loaded into all the required processors of the parallel machine. But it is mainly expected to be accurate for steady-state computations (actually, it is often used with steady-state codes [10]). Obtaining an accurate solution during the whole unsteady integration would require a local convergence (therefore an iterative process) at each time step.

In the parallel approach (Fig. 3), the two solvers are run together (in parallel) once the boundary conditions have been updated at their interface (at a coupling step). The fluid and solid domains are independently solved during a cycle of duration Δt (which is the coupling period, Fig. 3(a)). The time steps δt_F and δt_S are not necessarily equal. A cycle involves a coupling step and the subsequent integration of the fluid and solid domains (until the following exchange). Δt is thus a global time step linked to the coupled calculation, whereas δt_F and δt_S are related to the independent solver computations. Δt is chosen after the physics of the problem in order to reach a satisfactory trade-off between accuracy and time resolution. This point will be addressed in Section 5. The stability of coupling processes is a particular problem discussed in reference [17]. For instance, the condition that Δt must fulfil is different from the usual CFL or Fourier conditions.

In the general approach investigated in the current paper, the coupling step has two components. First, the interface conditions are computed from data provided by both solvers at the end of each cycle. Second, boundary conditions are assigned to the solvers. In Duchaine's parallel method, the first step is skipped and the solvers directly exchange their temperature and flux conditions at the boundary.

As discussed in Duchaine's article [15], the parallel coupling strategy is recommended for unsteady problems. It is all the more efficient in terms of computational cost as Δt is large (which reduces the frequency of exchanges between the solvers). The frequency of coupling steps influences the stability, the accuracy and the restitution time of the computation.

The parallel coupling strategy is thus selected for the current method. But three aspects of the coupling must still be specified:

1. the exact type of boundary conditions used by the two solvers at the interface. This defines a couple of boundary conditions, which will be specified in Section 3.2.2;
2. the way the interface conditions are computed, or, in other words, the selection of the interpolation scheme. This point will be addressed in Sections 3.2.1 and 3.2.3 (as well as in Section 4.1, in the case of the Finite Volume Method);
3. the method that ensures conservativity (Fig. 3(b)), which will be explained in Section 3.3 (and in Section 4.2 in the specific case of the Finite Volume Method).

The coupling strategy will have to be accurate, stable and conservative while using as large Δt as possible. The stress will be put on the constraints that will ensure these properties.

3.2. Constraints and purpose

3.2.1. Consistency

Consistency is an important property of numerical methods for conservation laws such as Eq. (1). $\vec{\nabla}(\vec{F}(U))$ is computed by using a numerical scheme. For instance, in a 1D form for illustration, at point i [18],

$$\frac{\partial \vec{F}(U)}{\partial x} \simeq \frac{\vec{F}^*_{i+1/2}(U_{i+k}, U_{i-k+1}, k \in \{1,\dots,N\}) - \vec{F}^*_{i-1/2}(U_{i-1+k}, U_{i-k}, k \in \{1,\dots,N\})}{\delta x}, \tag{5}$$

where δx is the grid cell size, $N \in \mathbb{N}^*$ and $\vec{F}^*$ is called the numerical flux (whereas $\vec{F}$ is the physical flux). $\vec{F}^*$ is a function of the values of U at the neighboring points. The consistency condition states that [18]

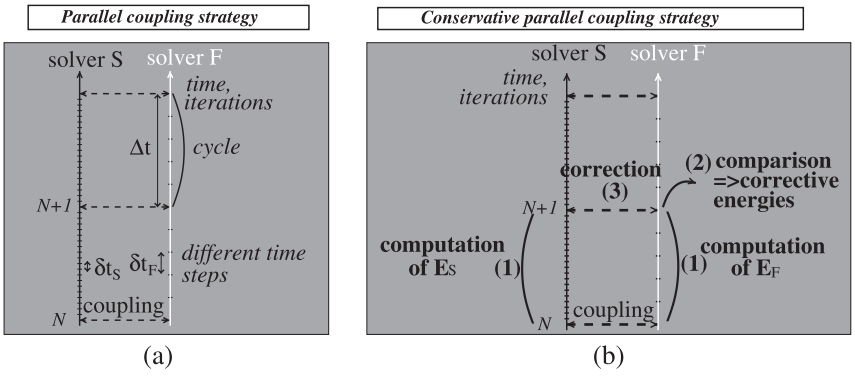

Fig. 3. Parallel coupling strategy.

$$\vec{F}^{*}_{i+1/2}(U_{i+k}, U_{i-k+1}, k \in \{1,\dots,N\}) = \vec{F}(U(x_{i+1/2})) \quad \text{when } \forall k, \quad U_{i+k} = U_{i-k+1} = U, \tag{6}$$

This condition ensures the consistency of Eq. (5) with the original Eq. (1).

Likewise, if Φ_0 and T_0 are arbitrary values of heat flux and temperature, a consistency condition can be designed for the interpolation scheme as:

$$\begin{cases} |\,\mathcal{F}_{\Phi}(\Phi_S,\Phi_F,T_S,T_F)\,| = |\,\Phi_0\,| \\ \mathcal{F}_T(\Phi_S,\Phi_F,T_S,T_F) = T_0 \end{cases} \text{when } \Phi_S = -\Phi_F = \Phi_0 \text{ and } T_S = T_F = T_0. \tag{7}$$

It ensures that an infinitely small discretization produces correct results. It also ensures that the state of equilibrium is stable once it has been reached, because the equilibrium temperature and heat flux remain enforced at the interface. The interpolation schemes which satisfy condition (7) must be recommended.

3.2.2. Coupling boundary conditions

Once the conditions Φ_I and T_I have been computed using Eq. (4), the boundary condition can be applied at the interface as a Neumann condition (Φ_I is enforced), as a Dirichlet condition (T_I is enforced) or even as a Robin condition (with a heat transfer coefficient h_I, a reference temperature $T_{I,\text{ref}}$ and a reference flux $\Phi_{I,\text{ref}}$). $h_I, T_{I,\text{ref}}$ and $\Phi_{I,\text{ref}}$ must fulfil the condition

$$\Phi_I = h_I(T_I - T_{I,\text{ref}}) + \Phi_{I,\text{ref}}. \tag{8}$$

More specifically, a couple of boundary conditions must be enforced (one condition per domain). Some authors [5,19] have selected the couple of boundary conditions at the solid/fluid interface as follows: the heat flux of the fluid is assigned to the solid and conversely the temperature of the solid is assigned to the fluid. Hence, the boundary conditions are a Neumann condition for the solid and a Dirichlet condition for the fluid. This option proves to be the most robust one in Giles' stability analysis [20]. To further improve the stability of the coupling process, a Robin condition is often preferred to the Neumann condition [7,9,15,21].

In the current paper, the notation for the two coupling boundary conditions will refer to the solid/fluid conditions, in that order: for instance, Robin/Dirichlet for a Robin condition assigned to the solid and a Dirichlet condition assigned to the fluid. It must be noted that the couple of boundary conditions is mainly selected on the basis of stability criteria [17].

3.2.3. Characteristics of unsteady coupling, influence of interpolation schemes

Steady coupling methods must at least ensure convergence to equilibrium of temperature and heat flux. For that purpose, the interpolation scheme must fulfil condition (7).

Extension to unsteady methods is not straightforward. Unsteady methods are expected to be accurate at each time of the computation. But a poor interpolation scheme induces errors which may vanish only once steady-state has been achieved. These errors may not even decrease over time if the computed case is purely unsteady.

As was explained earlier, a lot of methods found in the literature directly exchange their temperature and heat flux at the interface (Neumann/Dirichlet [5,19] or Robin/Dirichlet [7,9,15,21] boundary conditions), hence using a very basic "interpolation scheme". The following example will illustrate that such an inappropriate interpolation scheme induces a non-physical transient. Let us consider two coupled 1D domains whose initial temperatures T_1 and T_2 are uniform, in the solid and in the fluid, respectively (Fig. 4). At $t = 0s$, the uniform temperature in the fluid domain implies $\left(\vec{\nabla}T\right)_2 \cdot \vec{n} = 0$ and $\Phi_2 = 0$. Hence, using the Neumann/Dirichlet approach of the literature, the boundary condition is $\Phi_I = \Phi_{I,F}(t = 0s) = \Phi_2 = 0$ on the solid side of the interface. On the fluid side, it is $T_I = T_{I,S}(t = 0s) = T_1$. Φ_I is thus largely underestimated (the real value is infinite). But it is also very different from the heat flux computed during the subsequent fluid integration, which is for instance with a first-order scheme: $\lambda_F \frac{T_2 - T_1}{d/2} \neq 0$ (where d is the size of the first cell at the interface on the fluid side, as shown in Fig. 4). Thus, evaluating interface conditions in that way can introduce major errors which at least affect unsteady accuracy.

Actually, the interpolation scheme $\mathcal{F}$ must be as consistent as possible with the spatial schemes used by the solid and fluid solvers. It is now assumed that $\mathcal{F}$ is exactly inferred from the schemes of the solvers. If the solvers have equal time steps and are coupled at each time step ($\Delta t = \delta t_F = \delta t_S$), there is no mismatch between the heat fluxes at the surfaces of the two domains. Consequently, the heat flux is conserved and perfect equilibrium is achieved during the whole integration. But if $\delta t_F \neq \delta t_S$, the two domains are independently solved between two consecutive coupling steps (Fig. 3(a)). Therefore, regardless of the selected couple of boundary conditions, temperature and heat flux usually cannot be continuous at the interface all along the integration.

In the coupling method described hereafter, $\mathcal{F}$ is expected to be accurate by simultaneously and instantaneously balancing both temperature and heat flux at the interface. Derivation of $\mathcal{F}$ will be extensively discussed in the framework of the Finite Volume Method (Section 4.1.2, Eq. (16)).

3.3. A method for conservative coupling

Reference [17] has demonstrated that a non-conservative approach could result in significant errors in the steady-state computation of cases where Neumann conditions are assigned at all external boundaries and where at least one of the coupling boundary conditions is not a Neumann condition (which is often the case, at least for ensuring stability). It will be shown that using a conservative coupling method can also improve the accuracy of unsteady simulations (Section 5).

Let us assume that one of the coupling boundary conditions is not a Neumann condition. During the independent integrations of the two domains, the heat fluxes may be different on the two sides of the solid/fluid interface. This will produce energy losses. Indeed, the heat flux is enforced at the interface (and therefore equal on both sides) during the whole cycle only if Neumann conditions are assigned to both solvers. A corrective method is constructed to prevent such energy losses. This method, depicted in Fig. 3(b), consists of three steps:

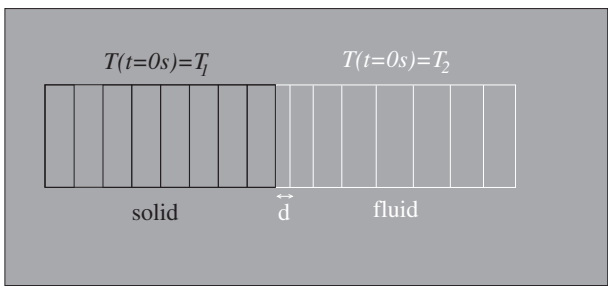

Fig. 4. Fluid and solid domains with uniform initial temperatures.

1. the computation of the transferred energies: the solvers compute the thermal energy transferred across each face of the interface during a cycle (solid: E_S, and fluid: E_F):

$$\begin{aligned} E_S &= \int_t^{t+\Delta t} \int_{\mathcal{S}} \overrightarrow{\Phi}_{I,S}(t) \cdot d\mathcal{S}\vec{n}dt, \\ E_F &= \int_t^{t+\Delta t} \int_{\mathcal{S}} \overrightarrow{\Phi}_{I,F}(t) \cdot d\mathcal{S}\vec{n}dt. \end{aligned} \tag{9}$$

$\vec{n}$ is the surface normal, $\mathcal{S}$ is the face area. If energy was conserved during the whole cycle, $E_S = -E_F$;

2. the computation of the conservative correction: at the coupling step, transferred energies E_S and E_F are compared face by face. The real amount of energy transferred across the interface (which is most probably neither E_S nor E_F) is not known and must be estimated. As shown in Fig. 5, the estimator E_I is interpolated as follows: $E_I = kE_S + (1-k)(-E_F)$. The weighting coefficient k takes values within the range $[0, 1]$. Corrective energies are inferred:

$$\begin{aligned} \Delta E_S &= E_I - E_S = (k-1)(E_S + E_F), \\ \Delta(-E_F) &= -\Delta(E_F) = E_I - (-E_F) = k(E_S + E_F); \end{aligned} \tag{10}$$

3. the assignment of the correction: the corrective energies ΔE_S and ΔE_F can be assigned either as flux conditions at the interface or as increments of temperature like $\Delta T_S = -\dfrac{\Delta E_S}{\rho_S c_S \mathcal{V}_S}$ (for instance in the adjacent cells of volume $\mathcal{V}_S$ in the solid, in the framework of the Finite Volume Method). Besides, ΔE_S and ΔE_F can be applied before or after updating the coupling boundary conditions. They can even be distributed over a given number of iterations of the following cycle. These options are called `pre-update`, `post-update` and `distributed` corrections, respectively (Fig. 6).

Consequently, the corrective energy is spatially (through the use of k) and temporally distributed. There are several ways to make these distributions. All of them ensure conservativity and improved accuracy but they are discriminated by their impact on stability.

Step 1 requires that the solvers compute the thermal energy transferred across each face of the interface during a cycle. It may be an intrusive part of the coupling method: integration of E (Eq. (9)) must be implemented into the solvers. Step 3 can also be intrusive, as will be seen in the case of the Finite Volume Method (Section 4.2).

4. The case of the Finite Volume Method

The solvers used in this study are based on the Finite Volume Method. The details of an efficient coupling scheme will be given in this framework.

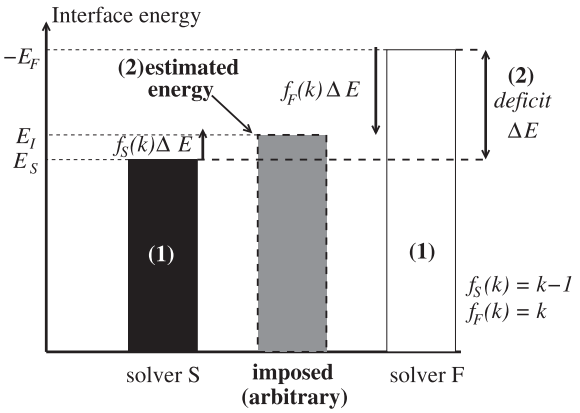

Fig. 5. Correction method: estimation of the corrective energy.

The Finite Volume Method is a broadly used discretization technique. It is designed to solve conservation equations such as Eq. (1) on structured or unstructured meshes in a conservative way. For any further information about this method, the interested reader will refer to [18] for example.

4.1. Interface boundary condition

Let us consider a face f at the interface, in the case of matching meshes (Fig. 1). S_n and F_n are the centroids of the adjacent cells in the solid and fluid domains, respectively. I is the centroid of face f.

The interface boundary conditions are computed at the coupling steps. Preliminary conditions are assessed at the end of the previous cycle, either at the cell centroids $\left(T^0_{S_n}, T^0_{F_n}\right)$ or at the interface ($T^0_{I,S}, \Phi^0_{I,S}, T^0_{I,F}, \Phi^0_{I,F}$, see Fig. 1). In general, $T^0_{I,S} \neq T^0_{I,F}$ and $\left|\Phi^0_{I,S}\right| \neq \left|\Phi^0_{I,F}\right|$ because of the independent computations of the solid and fluid domains during a cycle. The coupling method calls an interpolation scheme, which will be specified in the current section, to compute a single couple of values for temperature (T_I) and heat flux (Φ_I) at the interface.

4.1.1. Assumptions

To derive relevant estimators of T_I and Φ_I, a simplified typical case is addressed. Thus, the current interpolation scheme is based on two simplifying assumptions:

1. no wall function is used to solve the fluid. It means that either the flow is laminar or the grid is fine enough to ensure that F_n lies in the linear region of the thermal boundary layer ($y^+ < 5$, where y^+ is the wall coordinate of the first grid point [22]). The method could be improved to cope with more general flows and grids. A possible approach would consist in using an equivalent fluid conductivity, which would be computed from the heat flux provided by the wall function and from the gradient of temperature in the fluid. This would, however, require further investigation and is beyond the scope of this paper;
2. a first-order approximation is used to express the normal heat fluxes $\Phi^n_{I,S}$ and $\Phi^n_{I,F}$ at the interface at time level n. For instance, it is possible to write the vector flux $\overrightarrow{\Phi}^n_{I,S} = -\lambda_S \dfrac{T^n_{I,S} - T^n_{S_n}}{\left\|\overrightarrow{S_nI}\right\|} \dfrac{\overrightarrow{S_nI}}{\left\|\overrightarrow{S_nI}\right\|} + \delta\overrightarrow{\Phi}_S$, where the first term is the flux directed from the cell centroid to the interface centroid. The remainder $\delta\overrightarrow{\Phi}_S$ cannot be easily determined since it depends on the "non-aligned" temperature gradient (but it vanishes in a purely 1D approach for instance). Thus, using the distances $d_S = \dfrac{\overrightarrow{S_nI} \cdot \overrightarrow{S_nI}}{|\overrightarrow{S_nI} \cdot \vec{n}|}$ and $d_F = \dfrac{\overrightarrow{F_nI} \cdot \overrightarrow{F_nI}}{|\overrightarrow{F_nI} \cdot \vec{n}|}$ and the heat conductances $h_S = \dfrac{\lambda_S}{d_S}$ and $h_F = \dfrac{\lambda_F}{d_F}$ to simplify the equations yields

$$\begin{cases} \Phi^n_{I,S} \simeq -\lambda_S \frac{T^n_{I,S} - T^n_{S_n}}{d_S} = -h_S\left(T^n_{I,S} - T^n_{S_n}\right), \\ \Phi^n_{I,F} \simeq -\lambda_F \frac{T^n_{I,F} - T^n_{F_n}}{d_F} = -h_F\left(T^n_{I,F} - T^n_{F_n}\right). \end{cases} \tag{11}$$

The purpose here is to make a first step towards the use of a proper interpolation scheme for coupling methods. These assumptions will provide simple expressions for interpolation scheme $\mathcal{F}$. This approach is less accurate than if a higher-order approximation was used (or if wall functions were accounted for). But Section 5 will show that it is already far more accurate than usual approaches.

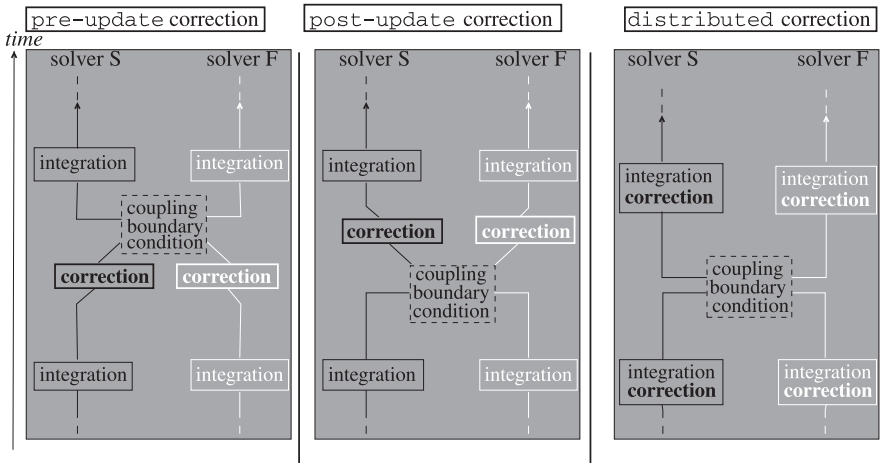

Fig. 6. Distribution of conservative correction over time.

4.1.2. Proposed interpolation scheme

The purpose of the interpolation scheme is to enforce Eq. (3), hence to update the values of temperature T_I and heat flux Φ_I at the interface so that, at the coupling step $n = 1$ (which is the beginning of the first iteration of the cycle), $T^1_{I,S} = T^1_{I,F} = T_I$ and $\Phi^1_{I,S} = -\Phi^1_{I,F} = \Phi_I$. Thus at $n = 1$, given preliminary conditions provided by the coupled solvers $T^1_{S_n} \leftarrow T^0_{S_n}$ and $T^1_{F_n} \leftarrow T^0_{F_n}$, these updated interface values still satisfy Eq. (11) if

$$\Phi_I = -h_S\left(T_I - T^0_{S_n}\right) = h_F\left(T_I - T^0_{F_n}\right), \tag{12}$$

which implies that

$$T_I = \frac{h_S T^0_{S_n} + h_F T^0_{F_n}}{h_S + h_F}. \tag{13}$$

Additionally, by eliminating $T^0_{S_n}$ and $T^0_{F_n}$ thanks to Eq. (11), Eq. (13) yields

$$T_I = \frac{h_S T^0_{I,S} + h_F T^0_{I,F} + \Phi^0_{I,F} + \Phi^0_{I,S}}{h_S + h_F}. \tag{14}$$

It must be noted that $\Phi^0_{I,F}$ and $\Phi^0_{I,S}$ are produced by the coupled solvers. Thus, they account for the complete temperature gradient as accurately as the numerical schemes permit (and they do not depend on the approximated expressions of Eq. (11)). Eventually, a good estimator of the heat flux at the interface is obtained by eliminating T_I in Eq. (12):

$$\begin{aligned}\Phi_I &= \tfrac{h_S h_F}{(h_S+h_F)}\left(T^0_{S_n} - T^0_{F_n}\right)\\ &= \tfrac{h_S h_F}{(h_S+h_F)}\left(T^0_{I,S} - T^0_{I,F}\right) + \tfrac{h_S h_F}{(h_S+h_F)}\left(\tfrac{\Phi^0_{I,S}}{h_F} - \tfrac{\Phi^0_{I,F}}{h_S}\right).\end{aligned} \tag{15}$$

Interpolation scheme $\mathcal{F}$ is therefore inferred from Eqs. (4), (14) and (15):

$$\begin{cases}\mathcal{F}_\Phi\left(\Phi^0_{I,S}, \Phi^0_{I,F}, T^0_{I,S}, T^0_{I,F}\right) = \tfrac{h_S h_F}{(h_S+h_F)}\left(T^0_{I,S} - T^0_{I,F} + \tfrac{\Phi^0_{I,S}}{h_F} - \tfrac{\Phi^0_{I,F}}{h_S}\right),\\ \mathcal{F}_T\left(\Phi^0_{I,S}, \Phi^0_{I,F}, T^0_{I,S}, T^0_{I,F}\right) = \tfrac{h_S T^0_{I,S} + h_F T^0_{I,F} + \Phi^0_{I,F} + \Phi^0_{I,S}}{h_S + h_F}.\end{cases} \tag{16}$$

Scheme $\mathcal{F}$ fulfils condition (7). T_I and Φ_I can be respectively assigned as Dirichlet and Neumann conditions (Φ_I for the solid, or $-\Phi_I$ for the fluid) at the interface until the following coupling step (that is at each iteration n of the cycle, although the derivation has been made, necessarily, at $n = 1$).

A Robin condition can also be computed, for instance in the solid domain, with

$$\text{or}\begin{cases} h_I = \frac{\Phi_I}{T_I - T^0_{F_n}} = h_F, & T_{I,\text{ref}} = T^0_{F_n}, \quad \Phi_{I,\text{ref}} = 0,\\ h_I = \frac{\Phi_I}{T_I - \left(T^0_{I,F} + \frac{\Phi^0_{I,F}}{h_F}\right)} = h_F, & T_{I,\text{ref}} = T^0_{I,F}, \quad \Phi_{I,\text{ref}} = -\Phi^0_{I,F}.\end{cases} \tag{17}$$

These expressions (which both have the same value for h_I) directly result from Eq. (8) with $\Phi_{I,\text{ref}} = 0$ and $T_{I,\text{ref}} = T^0_{F_n}$ in the first case and with $\Phi_{I,\text{ref}} = -\Phi^0_{I,F}$ and $T_{I,\text{ref}} = T^0_{I,F}$ in the second case.

Let N_S denote the number of iterations per cycle in the solid domain (which means that $\Delta t = N_S \delta t_S$), the boundary condition at the interface is ($\forall n \in \{1, N_S\}$)

$$\text{or}\begin{cases} T^n_{I,S} = T_I = \mathcal{F}_T(\Phi^0_{I,S}, \Phi^0_{I,F}, T^0_{I,S}, T^0_{I,F}) & \text{(Dirichlet)},\\ \Phi^n_{I,S} = \Phi_I = \mathcal{F}_\Phi(\Phi^0_{I,S}, \Phi^0_{I,F}, T^0_{I,S}, T^0_{I,F}) & \text{(Neumann)},\\ \Phi^n_{I,S} = -\Phi^0_{I,F} + & \\ \frac{\mathcal{F}_\Phi(\Phi^0_{I,S}, \Phi^0_{I,F}, T^0_{I,S}, T^0_{I,F})}{\mathcal{F}_T(\Phi^0_{I,S}, \Phi^0_{I,F}, T^0_{I,S}, T^0_{I,F}) - \left(T^0_{I,F} + \frac{\Phi^0_{I,F}}{h_F}\right)}\left(T^n_{I,S} - T^0_{I,F}\right) & \text{(Robin)}.\end{cases} \tag{18}$$

The same kind of relations can be obtained in the fluid domain.

4.1.3. Other possible interpolation schemes

Scheme based on the literature. $\mathcal{G}$ denotes here the scheme used by most authors, which is not based on a genuine interpolation. Indeed, the temperature of the solid domain is enforced at the fluid boundary and the heat flux of the fluid is assigned to the solid [5,19]:

$$\begin{cases}\mathcal{G}_\Phi\left(\Phi^0_{I,S}, \Phi^0_{I,F}, T^0_{I,S}, T^0_{I,F}\right) = \Phi^0_{I,F},\\ \mathcal{G}_T\left(\Phi^0_{I,S}, \Phi^0_{I,F}, T^0_{I,S}, T^0_{I,F}\right) = T^0_{I,S}.\end{cases} \tag{19}$$

Thus, the Robin/Dirichlet version of this usual method, which is most robust [7,9,15,21], reads

$$\text{and}\begin{cases}\forall n \in \{1, N_F\}, T^n_{I,F} = \mathcal{G}_T\left(\Phi^0_{I,S}, \Phi^0_{I,F}, T^0_{I,S}, T^0_{I,F}\right),\\ \forall n \in \{1, N_S\}, \Phi^n_{I,S} = \frac{\lambda_F}{d_F}\left(T^n_{I,S} - T^0_{F_n}\right).\end{cases} \tag{20}$$

Scheme $\mathcal{G}$ fulfils condition (7).

Scheme based on physical considerations. Another scheme can be designed according to the following physical law. Let β_F and β_S be the fluid and solid effusivities ($\beta = \sqrt{\lambda \rho c}$, where, for the fluid, c is the specific heat capacity at constant pressure, $c_{p_F} = \frac{\gamma r}{\gamma - 1}$). Then,

$$T_I = \frac{\beta_F T^0_{F_n} + \beta_S T^0_{S_n}}{\beta_F + \beta_S} \tag{21}$$

is the initial temperature at the interface of two semi-infinite walls of initial temperatures $T^0_{F_n}$ and $T^0_{S_n}$. This physical consideration does not allow to define a heat flux at the interface (whose initial value is infinite). Consequently, the interpolation scheme $\mathcal{H}$

$$\begin{cases} \mathcal{H}_\Phi\left(\Phi^0_{I,S}, \Phi^0_{I,F}, T^0_{S_n}, T^0_{F_n}\right) \text{ undefined}, \\ \mathcal{H}_T\left(\Phi^0_{I,S}, \Phi^0_{I,F}, T^0_{S_n}, T^0_{F_n}\right) = \frac{\beta_F T^0_{F_n} + \beta_S T^0_{S_n}}{\beta_F + \beta_S}, \end{cases} \tag{22}$$

can only be used with a Dirichlet/Dirichlet couple of boundary conditions:

$$\text{and} \begin{cases} \forall n \in \{1, N_F\}, T^n_{I,F} = \mathcal{H}_T\left(\Phi^0_{I,S}, \Phi^0_{I,F}, T^0_{S_n}, T^0_{F_n}\right), \\ \forall n \in \{1, N_S\}, T^n_{I,S} = \mathcal{H}_T\left(\Phi^0_{I,S}, \Phi^0_{I,F}, T^0_{S_n}, T^0_{F_n}\right). \end{cases} \tag{23}$$

Scheme $\mathcal{H}$ also fulfils condition (7).

The use of adiabatic wall temperature. In schemes $\mathcal{F}$, $\mathcal{G}$ and $\mathcal{H}$, the temperature of the fluid is assessed as a static temperature ($T^0_{F_n}$ or $T^0_{I,F}$). However, $\Phi = h(T_p - T_{aw})$ is the convective heat flux (with convection coefficient h) across a surface of temperature T_p, wetted by a flow of adiabatic wall temperature T_{aw}. It could therefore be attractive to use $T^0_{aw} = T^0_{F_n}\left(1 + C_r \frac{\gamma-1}{2}\left(M^0_{F_n}\right)^2\right)$ instead of the static temperature $T^0_{F_n}$ (C_r is the recovery factor, M_{F_n} is the Mach number in cell F_n). This would be especially true for Robin conditions.

If a coarse grid is used, the heat flux could be computed more accurately. If the grid is refined, T^0_{aw} is almost equal to $T^0_{F_n}$ because $M^0_{F_n}$ is small in the vicinity of the wall. The heat flux is then almost unaffected.

Nevertheless, C_r depends on the simulated case (geometry, laminar or turbulent flow). Moreover, using T^0_{aw} instead of $T^0_{F_n}$ may not improve the computation of T_I for all interpolation schemes. Eventually, in most cases, it may be better not to rely on this option to compensate for a poor mesh refinement.

Schemes $\mathcal{F}$ (which is recommend here) and $\mathcal{H}$ will be compared to scheme $\mathcal{G}$, which is usually used in the literature, in Section 5.6. Besides, the results produced by the use of static and adiabatic wall temperatures will illustrate the discussion of the current section.

4.2. The conservative correction method

The Finite Volume Method ensures conservativity inside the domains. The corrective method described in Section 3.3 allows conservative coupled computations. This method computes the corrective energies ΔE_S for the solid and ΔE_F for the fluid. ΔE_S and ΔE_F can be assigned as corrective increments of temperature in the adjacent cells (of volume $\mathcal{V}$): $\Delta T_{S_n} = -\frac{\Delta E_S}{\rho_S c_S \mathcal{V}_S}$ and $\Delta T_{F_n} = -\frac{\Delta E_F}{\rho_F c_{pF} \mathcal{V}_F}$. Directly adding ΔT to the temperature of the adjacent cell could require alteration to the fluid and solid solvers. The corrected version of the original scheme $\mathcal{F}$ (Eq. (18))

$$\begin{cases} T_I = \mathcal{F}_T\left(\Phi^0_{I,S}, \Phi^0_{I,F}, T^0_{I,S} + \Delta T_{S_n}, T^0_{I,F} + \Delta T_{F_n}\right), \\ \Phi_I = \mathcal{F}_\Phi\left(\Phi^0_{I,S}, \Phi^0_{I,F}, T^0_{I,S} + \Delta T_{S_n}, T^0_{I,F} + \Delta T_{F_n}\right), \\ h_I = \frac{\Phi_I}{T_I - \left(T^0_{I,F} + \frac{\Phi^0_{I,F}}{h_F} + \Delta T_{F_n}\right)}, \\ T_{I,\text{ref}} = T^0_{I,F} + \Delta T_{F_n}, \\ \Phi_{I,\text{ref}} = -\Phi^0_{I,F}, \end{cases} \tag{24}$$

is a less intrusive approach which achieves the `pre-update` correction (Fig. 6).

It is also possible to apply the correction as an additional heat flux at the interface. For a particular face (of area $\mathcal{S}$) at this interface, at each time step n,

$$\Phi^n_{I,S,c} = \frac{\Delta E_S}{\mathcal{S}\tau^n_c} \text{ and } \Phi^n_{I,F,c} = \frac{\Delta E_F}{\mathcal{S}\tau^n_c}, \tag{25}$$

where τ_c is a characteristic time. If $\forall n, \tau^n_c = \Delta t$ (duration of the cycle), the corrective energy is homogeneously distributed all along the cycle. An amount of energy $\frac{\delta t}{\Delta t}\Delta E$ is transferred at each time step of duration δt ($\Delta E = \Delta E_S$ in the solid or ΔE_F in the fluid). ΔE can also be distributed according to a geometric progression if at each step n, a proportion $\kappa \Delta E_n$ of the remaining energy $\Delta E_n = (1-\kappa)^{n-1}\Delta E$ is transferred. In this case, $\tau_c = \frac{\delta t}{\kappa(1-\kappa)^{n-1}}$ ($\kappa \in]0,1[$). The corrective fluxes thus read $\Phi^n_{I,S,c} = \frac{\kappa(1-\kappa)^{n-1}\Delta E_S}{\mathcal{S}\delta t}$ and $\Phi^n_{I,F,c} = \frac{\kappa(1-\kappa)^{n-1}\Delta E_F}{\mathcal{S}\delta t}$. The `post-update` correction is achieved for $\kappa = 1$: the whole corrective energy is assigned at the first iteration of the cycle.

$\Phi^n_{I,S,c}$ and $\Phi^n_{I,F,c}$ are added to the heat flux at the interface (for instance on the solid side and by using scheme $\mathcal{F}$) in the following way:

$$\text{or} \begin{cases} \forall n \in \{1, N_S\}, & \Phi^n_{I,S} = \mathcal{F}_\Phi(\Phi^0_{I,S}, \Phi^0_{I,F}, T^0_{I,S}, T^0_{I,F}) + \Phi^n_{I,S,c}, \\ \forall n \in \{1, N_S\}, & \Phi^n_{I,S} = \Phi^n_{I,S,c} - \Phi^0_{I,F} + \\ & \qquad \frac{\mathcal{F}_\Phi(\Phi^0_{I,S}, \Phi^0_{I,F}, T^0_{I,S}, T^0_{I,F})}{\mathcal{F}_T(\Phi^0_{I,S}, \Phi^0_{I,F}, T^0_{I,S}, T^0_{I,F}) - \left(T^0_{I,F} + \frac{\Phi^0_{I,F}}{h_F}\right)}\left(T^n_{I,S} - T^0_{I,F}\right), \end{cases} \tag{26}$$

which is a new corrected version of the Neumann and Robin conditions of Eq. (18). In the case of scheme $\mathcal{G}$, the same approach can be used to obtain a corrected version of the Robin condition of Eq. (20). This method implies that no Dirichlet condition is selected in the domain that receives the correction.

4.3. Coupling methodology

The coupling method must be stable and accurate. Stability is mainly linked to the selection of the couple of boundary conditions and to the parameters of the conservative correction method (spatial and temporal distribution). Indeed, a stability analysis which was partially presented in reference [17] shows that:

1. the couple of boundary conditions ensuring the most robust computations is: a Robin condition for the solid and a Dirichlet condition for the fluid. This observation is quite usual [7,20], except that, here, a conservative correction method is included;
2. the most robust corrective approach is provided by a `distributed` correction (Fig. 6) assigned as a heat flux on the solid side of the interface (and only on this side) as follows:

$$\Phi^n_{I,S,c} = \frac{\Delta E_S}{\mathcal{S}\Delta t} \quad \text{and} \quad \Phi^n_{I,F,c} = 0. \tag{27}$$

To that end, the weighting coefficient is $k = 0$, which means that the energy actually transferred across the interface during the cycle is computed on the fluid side (Fig. 5, Eq. (10)). Besides, the homogeneous temporal distribution of corrective energy is retained because it releases the whole energy the most robust

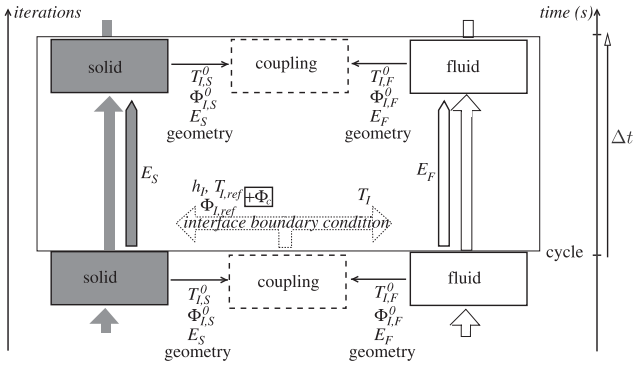

Fig. 7. Coupling methodology. $h_I = h_F$, $T_{I,ref} = T^0_{I,F}$, $\Phi_{I,ref} = -\Phi^0_{I,F}$.

way. It must ne noted that the `pre-update` and `post-update` corrections can produce slightly more accurate solutions than the `distributed` correction but they are less robust. As a consequence, the coupling boundary conditions are deduced from Eqs. (17), (18) and (27):

$$\text{and} \begin{cases} \forall n \in \{1, N_F\}, \quad T^n_{I,F} = \mathcal{F}_T\left(\Phi^0_{I,S}, \Phi^0_{I,F}, T^0_{I,S}, T^0_{I,F}\right), \\ \forall n \in \{1, N_S\}, \quad \Phi^n_{I,S} = h_F\left(T^n_{I,S} - T^0_{I,F}\right) - \Phi^0_{I,F} + \frac{\Delta E_S}{\delta \Delta t}, \end{cases} \tag{28}$$

and the global coupling methodology is depicted in Fig. 7. It must be pointed out that, apart from the calculation of the energy transferred across the interface during cycles (E_S and E_F), this methodology is not very intrusive into the solvers.

Considerations of accuracy determine the selection of scheme $\mathcal{F}$ and the use of a conservative approach in the current methodology, as will be illustrated in the following section.

5. Accuracy

The numerical results of the current method are compared with the analytical results provided by Pozzi et al. [1]. This test-case is intrinsically unsteady and is therefore appropriate to assess the accuracy of the current method.

5.1. Analytical case

In the considered analytical case, an infinite thick plate is wetted by a laminar flow impulsively accelerated to a constant Mach number M_∞. The physical parameters are: $M_\infty = 3$, $\Pr = 0.72, \gamma = 1.4, p = \dfrac{b\sqrt{\mathrm{Re}_\infty}\lambda_F(T_\infty)}{L\lambda_S} = 1, t_{fs} = \dfrac{\alpha_S}{b\left\|\vec{V}_\infty\right\|} = 1$ (α_S is the thermal diffusivity of the solid: $\alpha_S = \dfrac{\lambda_S}{\rho_S c_S}$) and $\theta_e = \dfrac{T_e - T_\infty}{T_\infty} = 2$. Pr and $\mathrm{Re}_\infty = \dfrac{\rho_\infty L\left\|\vec{V}_\infty\right\|}{\mu_F(T_\infty)}$ are the Prandtl and Reynolds numbers, respectively. b is the plate thickness and L is a characteristic length ($L = b$). $\left\|\vec{V}_\infty\right\|$ and T_∞ are the flow velocity and the temperature far from the plate. θ_e is the relative non-dimensional temperature enforced at the rear face of the thick plate (T_e is the dimensional temperature at this point). p and t_{fs} are two non-dimensional groups defined by Pozzi et al. as the main parameters of conjugate heat transfer problems.

Pozzi et al. obtained analytical results in compressible conditions thanks to the Stewartson - Dorodnitsyn transformation which requires a linear dependence of fluid thermal conductivity and viscosity with respect to temperature. As a consequence, $\mu_F(T) = \mu_\infty \dfrac{T}{T_\infty}$.

At $t = 0$ s, the flow Mach number suddenly becomes $M_\infty = 3$ and the temperature is $\theta_\infty = 0$ everywhere except at the rear face where $\theta_e = 2$. To compare the numerical approach to the analytical results, the main criterion will be the time-evolution of the non-dimensional temperature $\theta = \dfrac{T_I - T_\infty}{T_\infty}$ at the solid/fluid interface with respect to the non-dimensional time $\tau = \dfrac{t\left\|\vec{V}_\infty\right\|}{L}$. The numerical solution θ_n will thus be compared to the analytical solution [1]

$$\theta_a(\tau) = \theta_{w0}\left[1 - \vartheta\sum_{n=0}^{\infty}(-A)^n \operatorname{erfc}\left(\frac{n+1}{\sqrt{t_{fs}\tau}}\right)\right] + \vartheta\theta_e\sum_{n=0}^{\infty}(-A)^n \operatorname{erfc}\left(\frac{2n+1}{2\sqrt{t_{fs}\tau}}\right), \tag{29}$$

where $\theta_{w0} = \theta_{aw}\frac{\Lambda}{1+\Lambda}$ is the initial solution, $\theta_{aw} = 2\dfrac{\left\|\vec{V}_\infty\right\|^2}{c_{p_F}T_\infty}\dfrac{\arctan\left(\sqrt{\frac{2}{Pr}-1}\right)}{\sqrt{\frac{2}{Pr}-1}}$ is the non-dimensional adiabatic wall temperature, $\vartheta = \dfrac{2}{1+\Lambda}, A = \dfrac{1-\Lambda}{1+\Lambda}$ and $\Lambda = p\sqrt{t_{fs}}\sqrt{Pr}$.

5.2. Main parameters for the simulations

The method described in the current paper has been assessed on this test-case. The conservation laws (1) presented in Section 2.1 are numerically solved in the solid and fluid domains. The coupling method described in Section 4.3 is used to fulfil condition (3) at the interface of the solid and fluid domains. Then, unless explicitly specified, interpolation scheme $\mathcal{F}$ is used according to Eq. (28).

The simulations were performed at a pressure $P_\infty = 101325$ Pa and with $b = 0.05$ m, $T_\infty = 300$ K and $\mu_\infty = 1.808 \times 10^{-5}$ Pa s. An extrapolation condition was used at the top boundary of the fluid domain (Fig. 8). The semi-infinite geometry was modeled by the use of periodicity conditions at both left and right ends of the domain.

The computations were performed on three grids described in Table 1. The finest one is shown in Fig. 8. Due to the semi-infinite

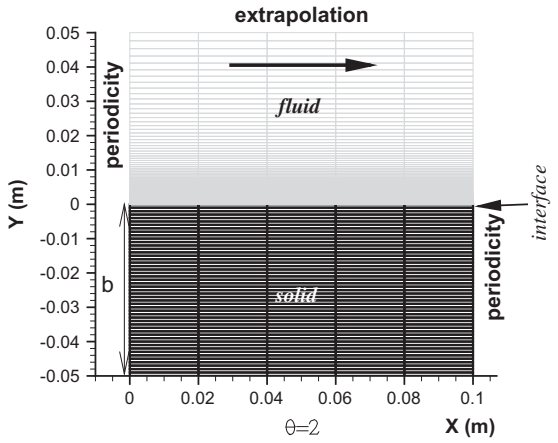

Fig. 8. Mesh for the verification case.

Table 1
Grids used for the computations.

Grid	Solid part		Fluid part	
	Number of points	Size, d_S (m)	Number of points	Size, d_F (m)
Fine	5×50	10^{-3}	5×244	$1.7 \cdot 10^{-8}$
Medium	5×5	10^{-2}	5×160	10^{-6}
Coarse	5×5	10^{-2}	5×40	$5 \cdot 10^{-5}$

configuration, only the transverse direction (Y) needs to be refined. There are five points in the streamwise direction for all three grids. The fluid and solid meshes were generated with matching nodes. The solid meshes are uniform (d_S is the cell size in the transverse direction). In the fluid domain, the cell size increases from the wall (d_F) to the far-field, according to a geometrical law of common ratio 1.05.

The flow was integrated with an explicit forward Euler method which admits a CFL condition $\sigma < 1$ [16]. Here, $\sigma = 0.6$. A first-order HLLC upwind scheme (Harten Lax Van Leer scheme, version by Toro [23]) was used. Time integration of the solid was also performed with an explicit method. Thus, the integration Fourier number $a = \dfrac{\alpha_S \delta t}{\delta x^2}$ must be smaller than 0.5. Here, $a = 0.4$.

No turbulence model was used, since the case is laminar. This prevents the problems discussed in Section 4.1.1, related to wall functions.

5.3. Influence of the grid refinement

The computations were performed on the three grids in case dt_0 (defined in Table 2). In this case, there is a single time step per cycle in both fluid and solid domains: $\Delta t = \delta t_F = \delta t_S$.

All the simulations with scheme $\mathcal{G}$ are rather inaccurate (Fig. 9(b)). For scheme $\mathcal{F}$, apart from a discrepancy in the early part of the computation, there is very little difference between the results on the fine and medium grids. As a consequence, most of the following discussion will be based on computations on the medium grid (which are cheaper). The simulations on the coarsest grid are clearly inaccurate, which disqualifies this mesh. It is also interesting to observe that, for the coarse grid, the results of schemes $\mathcal{F}$ and $\mathcal{G}$ are very similar.

Moreover, with scheme $\mathcal{F}$, the simulations on the fine and medium grids exhibit a non-physical peak of temperature in the first moments of the computation (Fig. 9(a)). The reason is linked to issues of grid cell size, as will be explained in the following section.

5.4. Resolution of the unsteady boundary layer

The thickness δ of the laminar boundary layer over an infinite flat plate theoretically increases over time (t) as follows [24]:

$$\delta \simeq 3.64\sqrt{\nu_F t}. \tag{30}$$

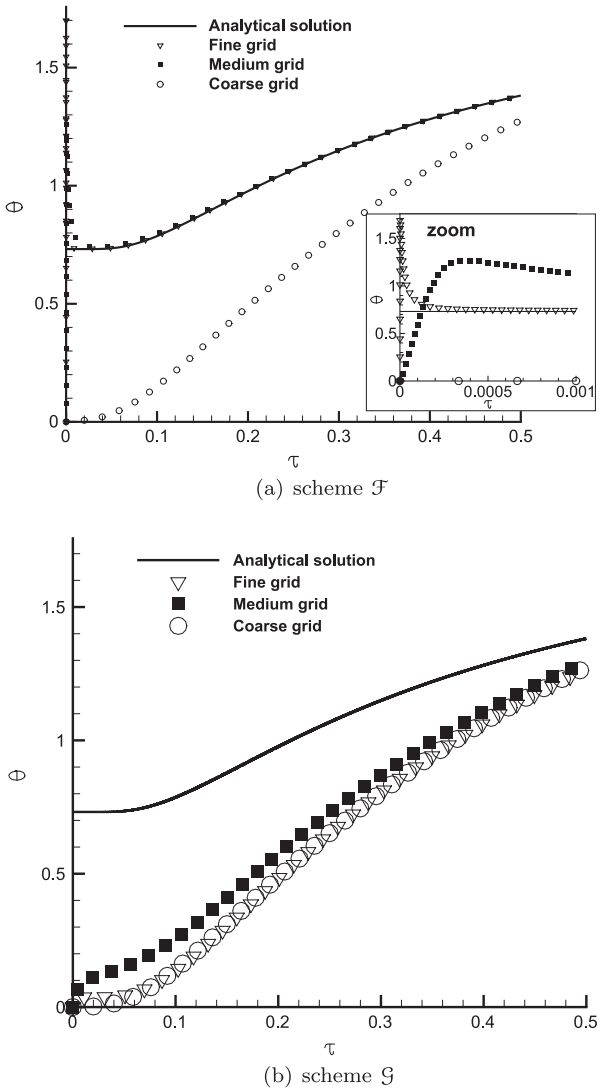

Fig. 9. Influence of the grid refinement, case dt_0.

$\nu_F = \frac{\mu_F}{\rho_F}$ is the kinematic viscosity of the fluid. Fig. 10 shows that the boundary layer is under-resolved in the beginning of all the computations: δ/d_F is smaller than 1, which means that the size of the first cell is larger than the boundary layer. For the coarse grid, this problem is encountered during almost the whole computation, which explains that the simulation cannot be accurate.

For the other grids, the bad resolution of the boundary layer is temporary and triggers peaks of temperature. For the medium grid, θ increases to 1.27 at $\tau = 3.7 \cdot 10^{-4}$, whereas the analytical solution is 0.73. At this time, $\delta \simeq 4d_F$ and $y^+ \simeq 3$ (also shown in Fig. 10). For

Table 2
Cycle time steps for the simulations.

	$\Delta t(s)$	Grid	$\Delta\tau$	Number of cells in the boundary layer at the end of the first cycle
dt_0	$5 \cdot 10^{-13}$	Fine	$9.37 \cdot 10^{-9}$	0
	$2 \cdot 10^{-10}$	Medium	$3.75 \cdot 10^{-6}$	0
	$1.6 \cdot 10^{-8}$	Coarse	$3.00 \cdot 10^{-4}$	0
dt_1	$3.2 \cdot 10^{-8}$	Medium	$6 \cdot 10^{-4}$	3
dt_2	$2.92 \cdot 10^{-7}$	Medium	$5.5 \cdot 10^{-3}$	7
dt_3	$3.2 \cdot 10^{-6}$	Medium	$6 \cdot 10^{-2}$	17

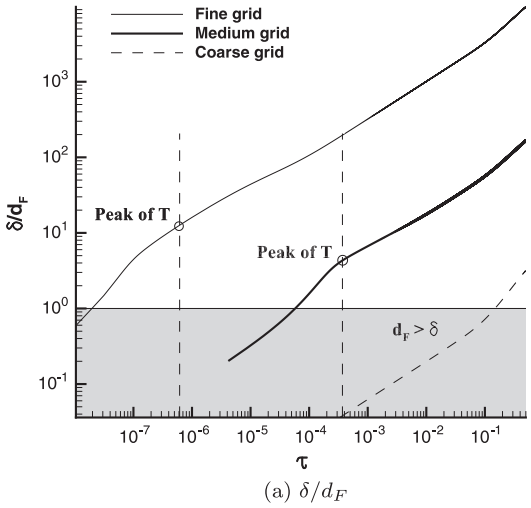

(a) δ/d_F

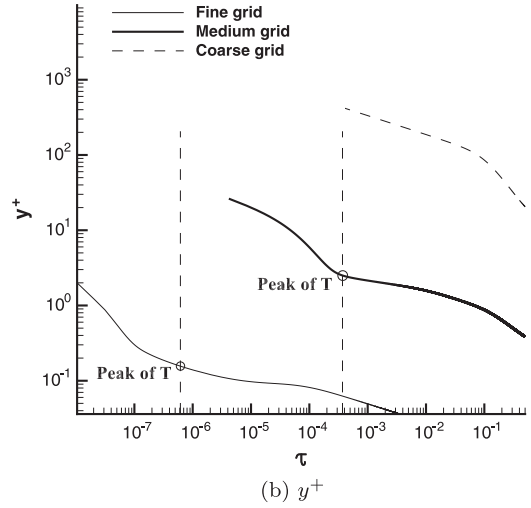

(b) y^+

Fig. 10. δ/d_F and y^+ with respect to non-dimensional time, case dt_0.

the fine grid, the phenomenon is restricted to very early times but the maximum value of θ is even larger, 1.77, at $\tau = 6.15 \cdot 10^{-7}$ ($\delta \simeq 13 d_F$ and $y^+ \simeq 0.16$). The numerical error decreases as the resolution of the boundary layer gets better (as δ/d_F increases or y^+ decreases). This study does not quantify a threshold value for δ/d_F and y^+, but at least a few points in the boundary layer seem to be required during the whole computation.

A major goal of the current paper is to assess the accuracy of our coupling method and to demonstrate that it is efficient. The following section will thus deal with the sensitivity of the results of this method with respect to several parameters. Moreover, the computations presented in Section 5.3 have already shown that our method is more accurate than the usual method (scheme $\mathcal{G}$). This point will be discussed more thoroughly in Section 5.6.

5.5. Influence of the duration of cycles and of the conservative correction

Figs. 11 and 12 show the influence of the coupling frequency on the accuracy of simulations. Dimensional and non-dimensional cycle durations (Δt and $\Delta\tau$) are provided in Table 2 for cases dt_0 to dt_3. Eq. (30) has been used to assess the number of cells included in the boundary layer at the end of the first cycle (which is also mentioned in Table 2). The problem of the temporarily under-resolved boundary layer, discussed in the previous section, was only encountered in case dt_0. In case dt_1, there are already three cells in the boundary layer at the end of the first cycle. Therefore, the peak of temperature does not occur (Fig. 11).

But as a counterpart, if the conservative correction method is not used, it is clear that increasing Δt from case dt_0 to case dt_3 leads to a significant reduction in the accuracy of the computation during the major part of the simulation (Fig. 12): the relative error $\varepsilon = \dfrac{\theta_n - \theta_a}{\theta_a}$ increases when Δt becomes larger.

The influence of the conservative corrections on accuracy is significant. Fig. 12 shows that, for the non-conservative approach, the relative error decreases by about one order from case dt_2 to case dt_1. But the accuracy of the conservative computation in case dt_2 and of the non-conservative simulation in case dt_1 is of the same order (although the coupling steps are around ten times less frequent in the second case). The same conclusion is given by the comparison between simulations dt_1 and dt_0. This test-case thus shows that the conservative method improves accuracy while reducing the frequency of the coupling steps.

5.6. Dependence on the scheme

The influence of the spatial discretization scheme has been assessed on the medium grid in case dt_1. For instance, using an AUSM scheme instead of an HLLC scheme does not significantly affect the results.

A major issue is the influence of the interpolation scheme. The computations with schemes $\mathcal{F}, \mathcal{G}$ and $\mathcal{H}$ (schemes presented in Sections 4.1.2 and 4.1.3) are compared in Fig. 13. The usual scheme ($\mathcal{G}$) has been tested with and without conservative corrections, even if most authors use a non-conservative approach. Fig. 13 shows that scheme $\mathcal{F}$ is the most accurate one. Besides, conservative corrections improve the results produced by scheme $\mathcal{G}$. It is also true for scheme $\mathcal{H}$, which is only slightly more accurate than scheme $\mathcal{G}$.

An additional remark is that the results produced by scheme $\mathcal{G}$ in case dt_0 are better on the medium grid than on the fine one (Fig. 9). Likewise, on the medium grid, scheme $\mathcal{G}$ is slightly more accurate in case dt_1 than in case dt_0. These counter-intuitive results are probably due to the low resolution of the boundary layer in the very beginning of the calculations. But a better understanding of this numerical behavior would require a thorough investigation which is beyond the scope of the current paper.

It should be pointed out that, although built after physical considerations, scheme $\mathcal{H}$ is less accurate than scheme $\mathcal{F}$. The problem is linked to an issue already raised in Section 4.1.3. Indeed, the analytical solution (Eq. (29)) shows that the initial temperature is

$$T_I(t=0\,\mathrm{s}) = \frac{\beta_F T_{aw}(t=0\,\mathrm{s}) + \beta_S T_S(t=0\,\mathrm{s})}{\beta_F + \beta_S} \neq \frac{\beta_F T_F(t=0\,\mathrm{s}) + \beta_S T_S(t=0\,\mathrm{s})}{\beta_F + \beta_S}, \tag{31}$$

which differs from Eq. (21) used for scheme $\mathcal{H}$ (Eq. (22)) because the adiabatic wall temperature T_{aw} must be used instead of the static temperature T_F. The poor accuracy of scheme $\mathcal{H}$ is thus mainly a consequence of the large flow velocity, which implies a noticeable difference between T_{aw} and T_F. Schemes $\mathcal{F}, \mathcal{G}$ and $\mathcal{H}$ usually do not account for this effect. Of course, none of them accurately assesses the initial interface temperature.

However, Fig. 14 shows that, as expected in Section 4.1.3, using T_{aw} does not systematically improve the accuracy of the simulations. The initial temperature produced by scheme $\mathcal{F}(\Phi^0_{I,S}, \Phi^0_{I,F}, T^0_{I,S}, T^0_{aw})$ is too large (whereas it is too small when using $\mathcal{F}\left(\Phi^0_{I,S}, \Phi^0_{I,F}, T^0_{I,S}, T^0_{I,F}\right)$). In general for scheme $\mathcal{F}$, using the static temperature produces slightly better results than using the adiabatic wall temperature.

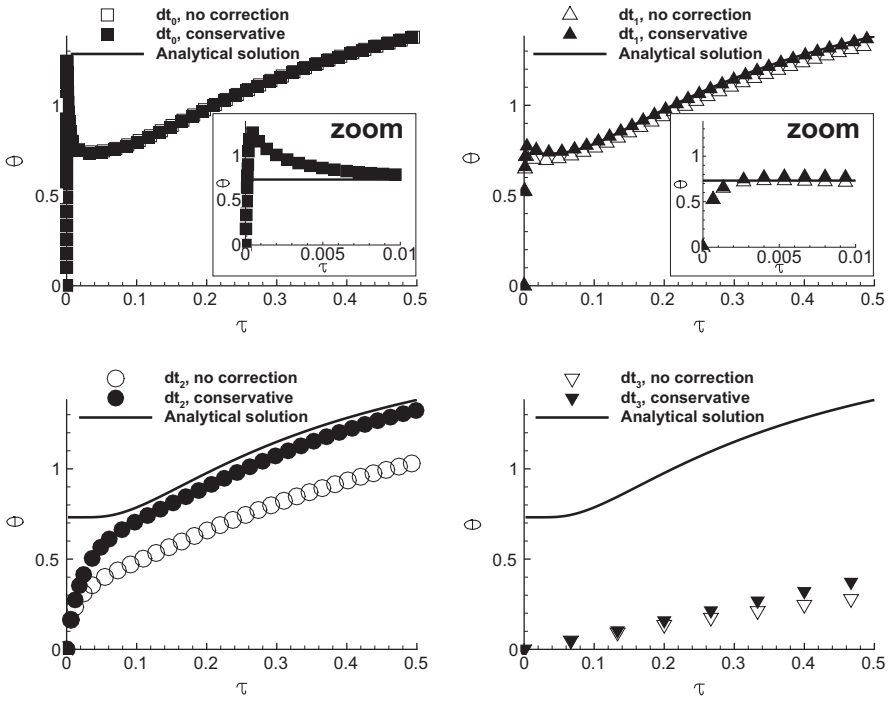

Fig. 11. Relative temperature at the solid/fluid interface with respect to reduced time: analytical and numerical results. Medium grid, scheme $\mathcal{F}$.

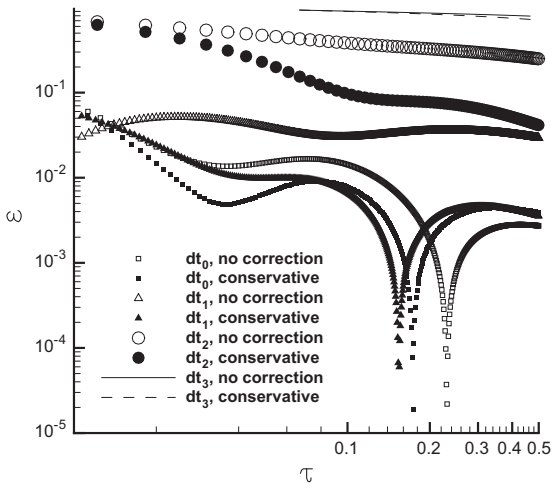

Fig. 12. Relative error in temperature at the interface. Medium grid, scheme $\mathcal{F}$.

On the contrary, $\mathcal{H}\left(\Phi^0_{I,S}, \Phi^0_{I,F}, T^0_{S_n}, T^0_{aw}\right)$ is slightly more accurate than $\mathcal{H}\left(\Phi^0_{I,S}, \Phi^0_{I,F}, T^0_{S_n}, T^0_{F_n}\right)$. The initial temperature is especially computed very accurately (as expected from Eq. (31)). However, regardless of the selected temperature, scheme $\mathcal{F}$ becomes more accurate than scheme $\mathcal{H}$ after a short time. Besides, the recovery factor for the laminar boundary layer over a flat plate has been inferred from Pozzi's paper [1]: $C_r = \dfrac{4\arctan\left(\sqrt{\frac{2}{Pr}-1}\right)}{\pi\sqrt{\frac{2}{Pr}-1}}$ (which is close to the usual value $\sqrt{Pr}$). But it must be recalled that C_r depends on the case.

It must also be noted that using T_{aw} instead of T_{F_n} does not noticeably change the results for scheme $\mathcal{G}$. This is not surprising: the use of T_{aw} was expected to especially affect Robin boundary conditions (Section 4.1.3). But whereas the Dirichlet boundary condition is affected by the use of T_{aw} in $\mathcal{G}_T$, the Robin boundary condition, which depends neither on $\mathcal{G}_T$ nor on $\mathcal{G}_\Phi$, remains unaffected (Eq. (20)).

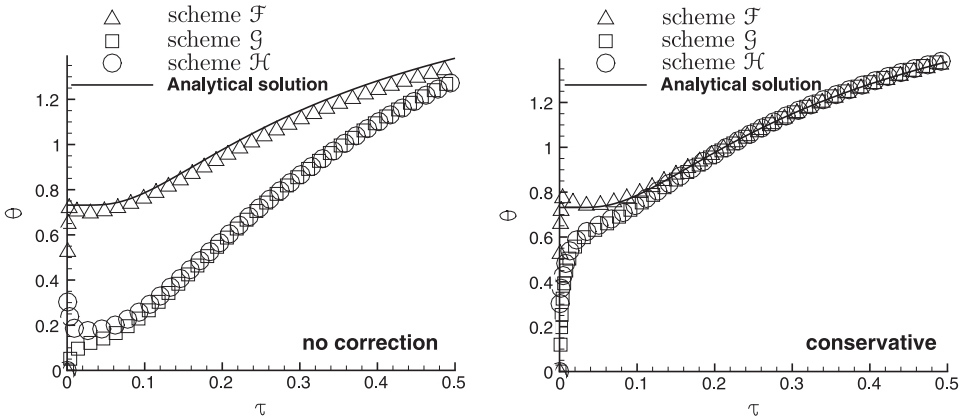

Fig. 13. Dependence on the interpolation scheme. Medium grid, case dt_1.

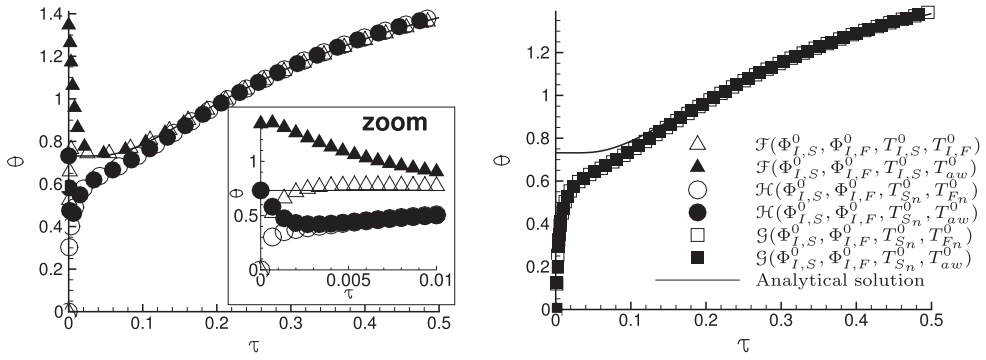

Fig. 14. Dependence on the selected temperature (static or adiabatic) for the fluid. Medium grid, conservative approach, case dt_1.

As a conclusion, all these comparisons show that scheme $\mathcal{F}$ (used with static temperature) is the most efficient interpolation scheme.

5.7. Main keys to successful coupled simulations

A poor accuracy of the fluid computation (for instance because of a temporary bad resolution of the boundary layer or because of turbulence [25]) leads to rather large errors in heat flux and temperature at the solid/fluid interface. For this reason, the duration of cycles Δt must not be too large compared to the physical duration of the phenomenon. For instance in case dt_3, although stable, the computation is not accurate at all (Fig. 11).

Δt must not be too small either. Indeed, if Δt is large enough, the temporal discretization of the two domains is limited by their own stability condition, which ensures optimal calculation for all solvers. Moreover, as already discussed by Duchaine et al. [15], decreasing the frequency of coupling steps allows to reduce the time consumed by coupling routines, and consequently to reduce the global computational cost. In the case discussed in this paper, the most appropriate option consists in using the cycle duration of case dt_1 along with conservative corrections. The results are as accurate as in case dt_0, although the number of coupling steps is 160 times smaller. Of course, the choice of Δt depends on the physics of the computed case. But this test-case shows that a conservative approach allows to increase the duration of cycles.

6. Conclusion

A methodology of numerical coupling has been developed for applications of unsteady conjugate heat transfer. It is mainly based on a parallel coupling strategy. The fluid and solid solvers are simultaneously run and the boundary conditions are periodically updated at their interface. This method is particularly efficient for unsteady computations, since it does not require the use of an iterative method at each time step. At the interface, the boundary conditions are usual (Dirichlet, Neumann or Robin). They are assigned a value given by an interpolation scheme which must fulfil a consistency condition. Several interpolation schemes have been defined and assessed in this article. The best scheme is consistent with the spatial discretization of the coupled solvers.

Moreover, heat flux is not strictly conserved at the solid/fluid interface. This is due to the independent behaviors of the solvers between the updates of their interface condition. A corrective method has been developed in order to maintain the intrinsic conservativity of the Finite Volume Method at the interface boundaries. The corrective process is based, first, on the evaluation of the difference between the heat fluxes on the two sides of the interface and, second, on the use of corrective fluxes.

To obtain a robust method, the fluid domains will usually receive a Dirichlet boundary condition at the interface and the solid domains will receive a Robin boundary condition. For the same reason, the whole corrective fluxes will also be assigned to the solid domains.

A verification of the coupling method has been carried out in this paper. In the case of an infinite thick plate wetted by a suddenly accelerated flow, evidence has been given that the proposed interpolation scheme is particularly efficient and that the conservative method leads to a significant gain in accuracy.

References

[1] Pozzi A, Tognaccini R. Time singularities in conjugated thermo-fluid-dynamic phenomena. J Fluid Mech 2005;538:361–76.

[2] Pozzi A, Tognaccini R. Coupling of conduction and convection past an impulsively started semi-infinite flat plate. Int J Heat Mass Trans 2000;43:1121–31.

[3] Fourcher B, Mansouri K. An approximate analytical solution to the Graetz problem with periodic inlet temperature. Int J Heat Fluid Flow 1997;18:229–35.

[4] Reulet P, Donjat D, Divouron E, Radenac E, Millan P. Infrared thermography analysis of the transient aerothermal evolution in a turbofan core compartment model. QIRT J 2009;6(2):225–48.

[5] Sondak DL, Dorney DJ. Simulation of coupled unsteady flow and heat conduction in turbine stage. J Propul Power 2000;16(6):1141–8. http://dx.doi.org/10.2514/2.5689.

[6] Li H, Kassab AJ. Numerical prediction of fluid flow and heat transfer in turbine blades with internal cooling. AIAA Paper, 94-2933; 1994.

[7] Heselhaus A, Vogel DT. Numerical simulation of turbine blade cooling with respect to blade heat conduction and inlet temperature profiles. AIAA Paper, 95-3041; 1995.

[8] Kao K-H, Liou M-S. Application of chimera/unstructured hybrid grids for conjugate heat transfer. AIAA J 1997;35(9):1472–8.

[9] Montenay A, Paté L, Duboué J-M. Conjugate heat transfer analysis of an engine internal cavity. ASME Paper, 2000, GT282; 2000.

[10] Verstraete T, Alsalihi Z, Van den Braembussche RA. Numerical study of the heat transfer in micro gas turbines. J Turbomach 2007;129(4):835–41. http://dx.doi.org/10.1115/1.2720874.

[11] Wang Q, Mathias EC, Heman JR, Smith CW. Gasdynamics and heat transfer modeling in rocket joints. J Spacecraft Rockets 2001;38(5):777–88.

[12] Hegab A, Jackson TL, Buckmaster J, Stewart DS. Nonsteady burning of periodic sandwich propellants with complete coupling between the solid and gas phases. Combust Flame 2001;125:1055–70.

[13] Urip E, Liew KH, Yang SL. Modeling IC engine conjugate heat transfer using the KIVA code. Numer Heat Trans A-Appl 2007;52:1–23.

[14] Rahaim CP, Kassab AJ, Cavalleri RJ. Coupled dual reciprocity boundary element/finite volume method for transient conjugate heat transfer. J Thermophys Heat Transfer 2000;14(1):27–38.

[15] Duchaine F, Corpron A, Pons L, Moureau V, Nicoud F, Poinsot T. Development and assessment of a coupled strategy for conjugate heat transfer with large eddy simulation: application to a cooled turbine blade. Int J Heat Fluid Flow 2009;30:1129–41.

[16] Hirsch C. Numerical computation of internal and external flows. Computational methods for inviscid and viscous flows. Fundamentals of numerical discretization, vol. 2. John Wiley and sons; 1990.

[17] Radenac E, Gressier J, Millan P, Giovannini A. A conservative coupling numerical method for transient conjugate heat transfer. In: International conference on computational methods for coupled problems in science and engineering, 25–28 May 2005, Santorini, Greece; 2005.

[18] Hirsch C. Numerical computation of internal and external flows. Fundamentals of numerical discretization, vol. 1. John Wiley and sons; 1998.

[19] Thakur S, Wright J. Conjugate heat transfer in a gas turbine blade trailing-edge cavity. AIAA Paper, 2002-0496; 2002.
[20] Giles MB. Stability analysis of numerical interface conditions in fluid-structure thermal analysis. Int J Numer Methods Fluids 1997;25(4):421–36. http://dx.doi.org/10.1002/(SICI)1097-0363(19970830)25:4<421::AID-FLD557>3.0.CO;2-J.
[21] Errera M-P, Baqué B. A quasi-dynamic procedure for coupled thermal simulations. Int J Numer Methods Fluids 2013;72(11):1183–206. http://dx.doi.org/10.1002/fld.3782.
[22] Schlichting H, Gersten K. Boundary-layer theory. 8th ed. Springer; 2000.
[23] Toro EF, Spruce M, Speares W. Restoration of the contact surface in the HLL-Riemann solver. Shock Waves 1994;4(1):25–34.
[24] White FM. Viscous fluid flow. 2nd ed. McGraw-Hill; 1991.
[25] Radenac E, Gressier J, Laroche E, Donjat D, Millan P. Couplage aérothermique et simulation de refroidissement par jet. Congrès Français de Thermique, SFT 2008, 03-06 Juin 2008, Toulouse, France; 2008.